Astronomy
&
Astrophysics

Rings in the haloes of planetary nebulae[*]

R. L. M. Corradi[1], P. Sánchez-Blázquez[2], G. Mellema[3,**], C. Gianmanco[4], and H. E. Schwarz[5]

[1] Isaac Newton Group of Telescopes, Ap. de Correos 321, 38700 Sta. Cruz de la Palma, Spain

[2] Departamento de Astrofísica, Universidad Complutense, 28040, Madrid, Spain
e-mail: pat@astrax.fis.ucm.es

[3] Sterrewacht Leiden, Postbus 9513, 2300 RA Leiden, The Netherlands
e-mail: mellema@strw.LeidenUniv.nl

[4] Instituto de Astrofísica de Canarias, 38200 La Laguna, Tenerife, Spain
e-mail: corrado@ll.iac.es

[5] Cerro Tololo Inter-American Observatory, NOAO-AURA, Casilla 603, La Serena, Chile
e-mail: hschwarz@ctio.noao.edu

Abstract. We present a search for rings or arcs in the haloes of planetary nebulae (PNe). We discovered such structures in eight PNe, tripling the sample of PNe with known rings. This shows that, contrary to what was believed to date, the occurrence of mass loss fluctuations with timescales of 10^2–10^3 yrs at the end of the asymptotic giant branch phase (AGB) is common. We estimate a lower limit of the occurrence rate of rings in PN haloes to be ∼35%.

Using these new detections and the cases previously known, we discuss the statistical properties of ring systems in PNe haloes. We estimate that the mass modulation producing the rings takes place during the last 10 000 or 20 000 yrs of AGB evolution. In PNe, the spacing between rings ranges from <0.01 pc to 0.06 pc, significantly larger than those seen in proto-PNe. This, together with the finding of a possible positive correlation of spacing with the post-AGB age of the nebulae, suggests that the spacing of the rings increases with time.

These properties, as well as the modest surface brightness amplitudes of rings, are consistent with the predictions of the dust-driven wind instability model explored by Meijerink et al. (2003), but do not immediately exclude other proposed models.

Key words. ISM: planetary nebulae: general – stars: AGB and post-AGB

1. Introduction

Most PNe have multiple shells around their central stars. Modern simulations allow us to interpret the formation of most of these shells. We know, for instance, that the typical double-shell structure of the bright inner body of round and elliptical PNe is the result of wind interaction (producing the so-called inner *rims*) and that photo-ionization effects are responsible for producing the attached *shells*. For a detailed discussion see e.g. Mellema (1994) and Schönberner et al. (1997).

Around the inner nebula, with 1000 times lower surface brightness, an extended ionized *halo* has been found in 60% of the PNe for which proper imaging has been obtained (Corradi et al. 2003, hereafter CSSP03). These haloes are interpreted as being matter lost at the end of the asymptotic giant branch (AGB) phase, their edges being the signature of the last thermal pulse (Steffen & Schönberner 2003).

In recent years, a new puzzling component has been discovered in the inner regions of PNe haloes. High resolution imaging done mainly with the Hubble Space Telescope has revealed the presence of so-called "rings" in four PNe: Hb 5, NGC 6543, NGC 7027 (Terzian & Hajian 2000), and NGC 3918 (CSSP03), as well as around six proto-PNe and one AGB star (see the review by Su 2004). The name "rings" is somewhat misleading in that these structures just appear to be rings when projected on the sky. They are more likely to be "shells". But since the nomenclature of morphological features in PNe is already somewhat confused, we will use what seems to be the most widely accepted name, namely "rings". Note that Soker (2002, 2004) refers to them as "M-arcs". Their formation, occurring when the star loses mass at the highest rate during its

---

Table 1. Log of the new observations.

Object	PNG	Telescope	Filter	Exp. time [s]	Seeing [arcsec]
NGC 40	120.0+09.8	INT	Hα+[NII]	60, 3600	1.1
NGC 1535	206.4–40.5	INT	[OIII]	30, 1200	1.5
NGC 3242	261.0+32.0	INT	[OIII]	30, 1800	1.6
NGC 6543	096.4+29.9	NOT	[OIII]	30, 120, 1800	0.8
NGC 7009	037.7–34.5	INT	[OIII]	10, 60, 300, 1200	1.4
		INT	Hα+[NII]	20, 180, 1200	1.3
		MPG/ESO	[OIII]	15, 90, 600	0.8
NGC 7027	084.9–03.4	NOT	[OIII]	10, 120, 300, 1800	0.8
NGC 7662	106.5–17.6	INT	[OIII]	20, 110, 600	0.8

evolution, is relevant to understanding the physical processes producing the ultimate ejection of the envelope of low- and intermediate-mass stars. To date, however, very little is known about the physical and dynamical properties of these rings, especially in the PNe phase where, so far, they were considered to be a rare phenomenon. In this paper, we present the results of an extensive search for such rings in PNe haloes. We find them in eight more PNe, showing that rings are quite common, and thus strengthening the idea that the physical processes producing the rings is of general importance to understand mass loss in the latest phase of the AGB.

2. Observations

The observational targets were mainly chosen from the list of PNe with haloes in CSSP03. The original images were carefully reanalysed, and for several targets for which hints of the existence of rings were found we obtained new deep images. It must be stressed that often the main limitation in searching for this kind of structures is not the spatial resolution of the observations, but the instrumental scattered light as discussed in CSSP03. For this reason, we obtained most of the new images with the prime-focus Wide Field Camera (WFC, pixel scale 0.″33) at the 2.5 m Isaac Newton Telescope (INT) at La Palma, which has a clean point-spread function. We obtained deep [OIII] and/or Hα+[NII] images. The [OIII] filter bandpass does not include any other important emission lines beside the [OIII] doublet at λ = 500.7 and 495.9 nm. The Hα+[NII] filter includes both the emission from hydrogen Hα and that from the singly ionized nitrogen doublet at λ = 654.8 and 658.3 nm. Exposures were split into several sub-exposures to limit the effects caused by over-saturation of the inner bright nebula (i.e. charge overflow). For the same reason we sometimes positioned the inner nebula in the gap between CCDs in the four-chip mosaic of the WFC. [OIII] images of NGC 7009 were also obtained with the Wide Field Imager (WFI, pixel scale 0.″24) of the 2.2 mMPG/ESO telescope at La Silla, Chile, under good seeing conditions. [OIII] images of NGC 6543 and NGC 7027 were obtained with the 2.6 m Nordic Optical

Telescope (NOT) at the ORM and its multi-mode instrument ALFOSC (pixel scale 0.″19). The images were reduced in a standard way using the IRAF and MIDAS packages. The observations with the INT+WFC were partially reduced by Greimel & Davenport through the instrument pipeline. A summary of the new observations is presented in Table 1.

In addition, the HST archive was searched for the deepest images of a number of nebulae known or suspected to have rings.

3. Image analysis: Finding and enhancing the rings

The new images clearly reveal the existence of rings in several of our target PNe. However, rings are not easily visualized in greyscale or colour plots, as they are located in the inner regions of the haloes whose surface brightness has a very steep radial profile with a large dynamic range. In order to better highlight the rings and measure their properties, we processed the images in several different ways. Good results are obtained by taking the logarithmic derivative of the images. This method is described in Corradi et al. (2004). An even better way to enhance the rings is to divide the original image by its smoothed version, using any kind of algorithm with a smoothing scale-length of the order of the rings spacing. We call this as the *smoothing* algorithm. Nearly identical results are obtained by processing images with what we call the *sda* (*shift*, *divide*, and *add*) algorithm. One first produces four "shift" images, by applying to the original frame $I(x, y)$ a shift of p pixels to the right, left, up and down, respectively. Then the original image is divided by each of the shift images, and the four ratio maps are summed up together producing the final image I_{sda}. In symbols:

$$I_{sda} = \frac{I(x,y)}{I(x-p,y)} + \frac{I(x,y)}{I(x+p,y)} + \frac{I(x,y)}{I(x,y-p)} + \frac{I(x,y)}{I(x,y+p)}.$$

In this way, pixels corresponding to the larger surface brightness of the rings are enhanced by division by an "average" surface brightness of the halo in that region. The *sda* procedure

Table 2. Rings properties in PNe. In the second column, *r* means "rings" and *a* "arcs". In the last column, we quote the adopted distance for each PN.

Object	N. of rings	Spacing [arcsec]	Peak-to-continuum ratio	Comments	Dist. [kpc]
Clear detections					
Hb 5[★]	6a	0.6–1.3	2	concentric	1.5
NGC 40	3r+2a	5.0–7.4	1.10	concentric	1.1
NGC 3242	3r+2a	6–10	1.12	concentric	0.8
NGC 3918	8r	2.0–6.6	1.07	concentric (except last)	1.2
NGC 6543[★]	>11r	2.2–3.8	1.2	concentric	1.0
NGC 7009	6r	2.9–4.8	1.09	non-circular, intersect?	0.9
NGC 7027[★]	>9r	2.2–5.8	1.5	incomplete, some intersecting	1.0
NGC 7662	4r	5.0–5.3	1.12	approx concentric	1.2
Probable detections					
IC 2448	3r	3.5–3.8	1.05	non-circular	1.4
NGC 1535	2r+1a	7.2–11.3	1.07	non-circular	1.8
NGC 6881	3a	1.0	–		3.2
NGC 7026	2a	2.5	–		1.6

[★]Data from Su (2004).

was tested in several ways, to make sure that no artificial rings are created by the algorithm and that the location of the rings remains the same. We created a model image with a r^{-3} surface brightness profile and, superimposed, sinusoidal fluctuations with amplitude 20% the value of the local intensity and period equal to 20 pixels, simulating a halo with rings. The *sda* algorithm was then applied using shifts $p = 10, 15, 20, 25, 30$ pix. For any choice of p, rings are effectively enhanced. The only spurious effect is the appearance, for shift values ≥ 20 pix, of slight distortions of the circular symmetry, but even in the directions where the effect is the largest, the original spacing between rings is always preserved with a high accuracy.

We processed with the three algorithms all the new ground-based images, as well as the [OIII] images of IC 2448, NGC 1535 and NGC 3918 from CSSP03, and the HST images of NGC 6881 (Hα) and NGC 7026 ([NII]). For the *sda* processing, according to the results of the tests, a shift value equal to or smaller than the average ring spacing was adopted. In all PNe, rings show up using any of the three algorithms (and except for IC 2448 and NGC 1535 they are also clearly detected in the non-processed images). Faint rings are better enhanced using the smoothing algorithm or the *sda* one, rather than taking derivative images. The *sda* algorithm, which produces nearly identical results to the smoothing method for the external regions, provides a better enhancement of the innermost ring, as smoothing in this region is affected by the abrupt change of slope of the surface brightness profile due to the nearby bright rim and shell.

Logarithmic greyscale displays of the original frames, the images processed using the *sda* algorithm, and visual fits of the detected rings are presented in Figs. 1 and 2.

4. Description of individual nebulae

The individual PNe are discussed below, and a summary of the properties of their ring systems (including objects discussed by Su 2004) is presented in Table 2.

4.1. IC 2448

CSSP03 conservatively put this object in the list of PNe with no haloes because of the possibility that the diffuse, featureless luminosity detected around the central body of the PN is instrumental scattered light. The processing of their original, high-quality [OIII] image (seeing 0″.6) reveals the presence of fluctuations of the radial surface brightness profile that can be roughly described as a system of three or more rings in an extended AGB halo. Rings are not as well defined as in other PNe, and show some sign of non-circularity and/or offsets from the central star.

4.2. NGC 40

In addition to the structure in the faint halo around this nebula, our deep Hα+[NII] image reveals the existence of a system of three concentric inner rings centred on the central star. Fragments of one or two external rings are also found. NGC 40 is a low excitation nebula, and no halo is visible in the [OIII] images.
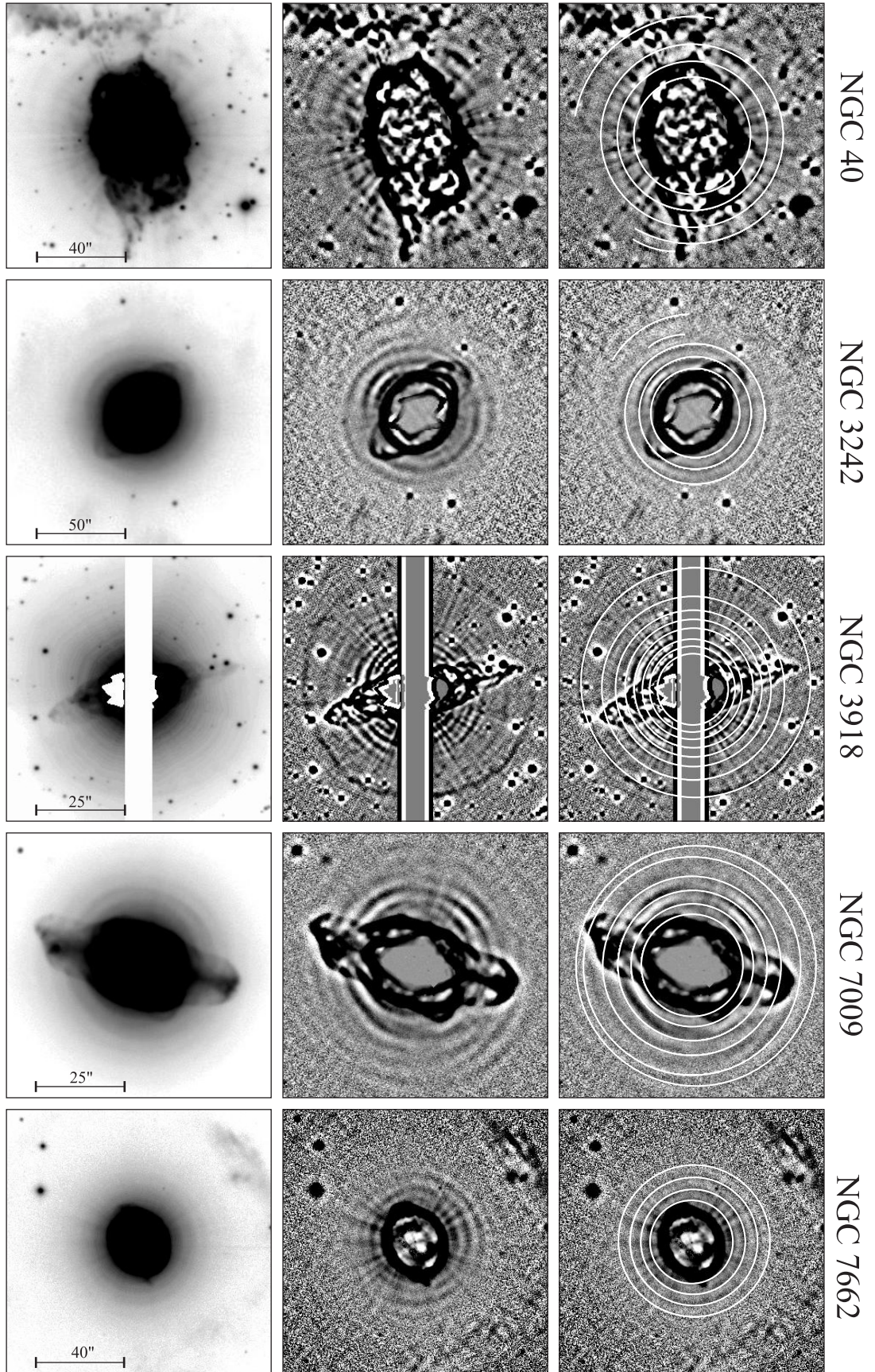
Fig. 1. Images of the definite new detections of rings. All images are displayed in *negative* greyscale (i.e. black means larger emission values). On the left, the original image in a logarithmic display, at the centre the *sda* processed image (see text) in a linear display, and to the right the same ones with superimposed a visual circular fit of the rings/arcs.
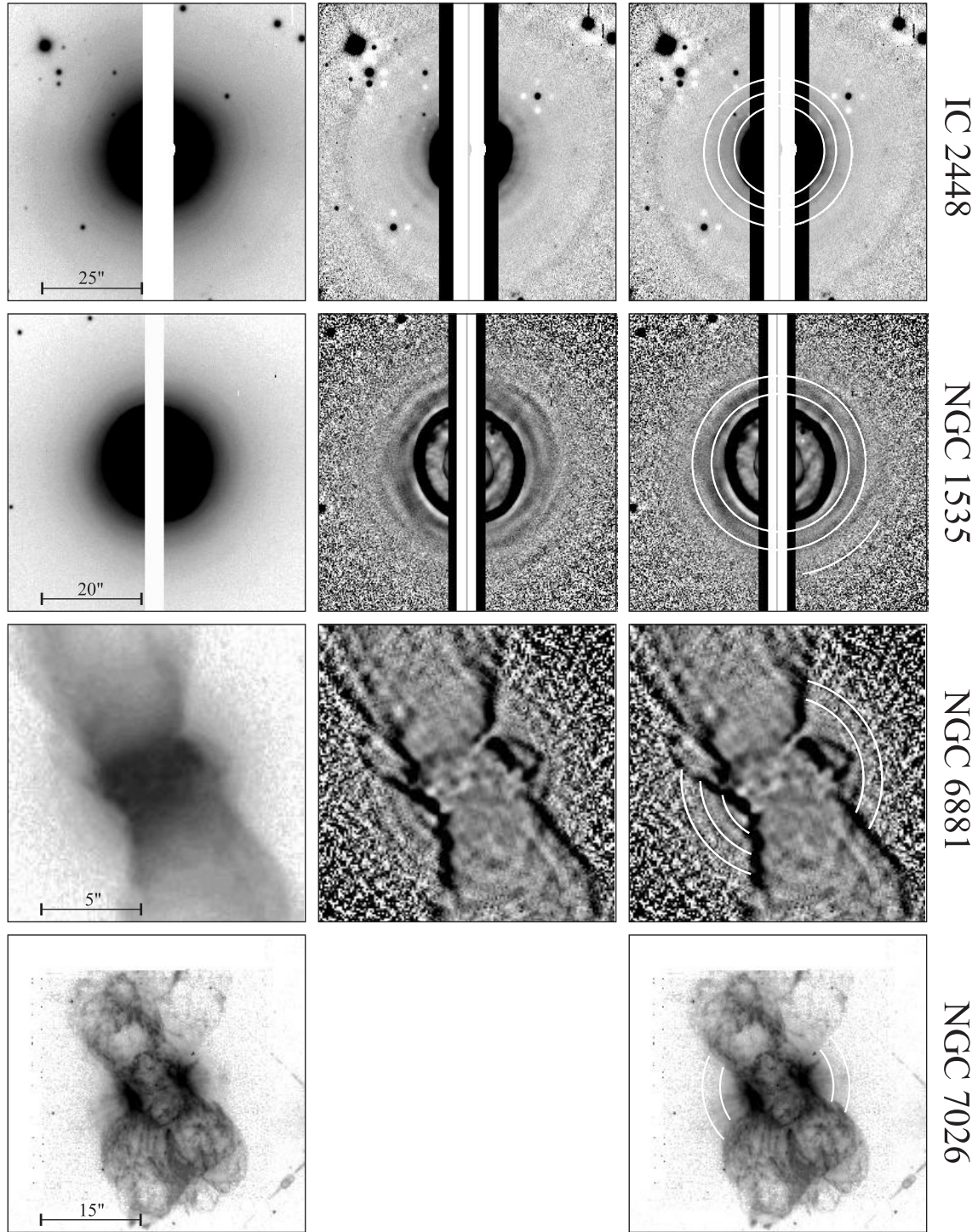
Fig. 2. As in Fig. 1, but for the PNe with probable detections of rings. For NGC 7026, no *sda* processed image is presented (see text).

4.3. NGC 1535

Processing of the original [OIII] image by CSSP03 (seeing 0.″6) reveals the presence of at least two rings and a fragment (arc) of an outer one. Rings are broad and non circular. A recent image taken with the INT+WFC, in spite of having a lower spatial resolution (seeing 1.″5), confirms the presence and properties

of such broad rings, thus excluding the possibility that they are instrumental artifacts.

4.4. NGC 3242

The [OIII] INT+WFC image shows three clear rings and fragments of two other outer ones. The innermost two rings are

faintly visible in archival HST images. The rings are concentric and the spacing between them is variable. They are also visible in the Hα+[NII] image by CSSP03.

4.5. NGC 3918

The rings in the halo of this nebula were noted by CSSP03. Data processing of their image confirms that there are at least 8 concentric circular rings with a spacing that increases from 2″ for the innermost ones, to 3″.8 for the second last one. The outermost ring is slightly offset by a couple of arcseconds to the North-West and has a radius 6″.6 larger than the preceding one (but we might be missing an intermediate ring). It also appears to be more intense than the previous few ones, defining a sharp edge of the system of rings. The actual edge of the AGB halo, presumably corresponding to the last thermal pulse, is at a much larger distance from the central star, see CSSP03.

4.6. NGC 6543

Our deep [OIII] images confirm the results of the detailed analysis of the HST data by Balick et al. (2001), with the possible addition of two more outer rings out to a distance of ~50″ from the central star. For this reason, our new images are not presented in Figs. 1 and 2.

4.7. NGC 6881

Three roughly circular, equally spaced arcs are barely visible in Hα HST archive images along the directions perpendicular to the bipolar lobes.

4.8. NGC 7009

The new INT and MPG ground-based images reveal the existence of at least six rings in the inner regions of the knotty halo of this PN. As in the other cases, rings are best visible in the *sda* processed image, and show clear deviations from the circular symmetry (in Fig. 1, a visual fit for the northern side of the nebula fits the southern side poorly), with possible intersection between adjacent rings. The spacing between the rings is variable.

4.9. NGC 7026

Two arcs (whose centre is slightly offset from the central star) are possibly identified in [NII] HST images, but this is the weakest case of all our new detections. This is in fact the only case in which our image processing does not enhance the possible rings, probably because of the highly structured local surface brightness distribution (including strong radial features).

4.10. NGC 7027

The reflection rings of this object were discussed by e.g. Su (2004). Our new deep [OIII] images (not presented in Figs. 1

and 2) confirm their results, showing evidence for a few other faint outer rings up to a distance from the central star of ~50″.

4.11. NGC 7662

A new, clear system of 4 rings is found in this PN. The rings are approximately concentric, but with some hints of non-circularity and offset from the central star (the latter for the outer rings).

5. General properties of rings

5.1. Detection rate

Rings are found in PNe of different morphological classes: elliptical nebulae (NGC 40, NGC 1535 and IC 2448), ellipticals with low-ionization small-scale structures like FLIERS (NGC 3242 and NGC 7662), more collimated nebulae with jets (NGC 3918, NGC 6543 and NGC 7009), and bipolars (Hb 5, NGC 6881, NGC 7026, and NGC 7027, the latter also probably bipolar, see Bains et al. 2003). Note also that some of the PNe with detected rings, namely NGC 40, NGC 6543 and NGC 7026 have hydrogen deficient central stars.

CSSP03 list 21 PNe possessing bona-fide AGB haloes. Including the haloes with rings revealed in this paper for IC 2448, NGC 40, and NGC 1535, this makes 24 non-bipolar PNe known to have AGB haloes. The present analysis of the CSSPO3 sample (including the new deep images and the HST archive ones) allowed us to discovered rings in 8 of these 24 PNe, i.e. some 35% of the sample of AGB haloes investigated. Considering that CSSP03 estimate that ≥60% of the whole sample of Galactic PNe have ionized AGB haloes, we derive that the lower limit for the frequency of rings in round and elliptical PNe is 20%. The real figure can be much higher, as high-quality images needed to detect rings (or even to reveal haloes) are not available for the whole CSSP03 sample. One is therefore tempted to ask whether rings exist in *all* PNe? The database of CSSP03 contains some haloes with no apparent evidence for rings. These are for example CN 1-5, IC 2165, NGC 2022, NGC 2792, NGC 6826 and PB4. Except for NGC 6826, however, all these PNe are located at systematically larger distances (several kpc) than those with detected rings, most of which lie at about 1 kpc from the Sun, see Table 2. This is also reflected by a systematically smaller apparent size of the haloes of PNe with no rings. The resolution in the ground-based images just may not be sufficient to detect rings in those distant PNe. We therefore conclude that the 35% occurrence rate in the present study is a lower limit, and the possibility that rings are present in the majority of or all PNe cannot be excluded.

The situation for bipolar PNe is more uncertain, as we do not even know whether this class of objects has AGB haloes, at least in the sense as defined by CSSP03. However, having found arcs in several objects, it is likely that also for this class of nebulae circular rings/arcs are common. Therefore bipolar lobes would excavate through pretty spherical initial circumstellar density distributions, exacerbating the problem of a sudden turn from spherical to highly collimated mass loss at the

end of the AGB (e.g. Sahai 2002). This is supported by the finding of rings and arcs in several *bipolar* proto-PNe (Su 2004). With the present data, we cannot say if the rings of Hb 5, NGC 6881 and NGC 7026 are seen in direct or reflected light as is the case in NGC 7027 and the proto-PNe.

5.2. Post-AGB and post-ionization ages

Some of the models proposed to explain the formation of rings predict that during the PN phase rings would persist only few thousand years after photo-ionization (Meijerink et al. 2003, hereafter MMS03). Unfortunately, measuring how long the ring systems have been photo-ionized is a hard task for individual PNe. In principle, this could be done if the luminosity and temperature of their central stars (CSs) are accurately known. A comparison with the theoretical tracks would then allow us to determine their stellar mass and post-AGB age. This is however extremely difficult to do, as the evolutionary timescales are strongly dependent on mass, which on the horizontal part of the post-AGB tracks mainly depends on luminosity, the determination of which suffers from the large uncertainties in the distance to individual PNe. We attempted this kind of analysis, using both the data from the CSs in CSSP03 and those from Mal'kov (1997), but for individual objects the results show large discrepancies between the two different data sets, making this kind of analysis impracticable. All we can conclude at present, in a statistical sense, is that PNe with rings do not exhibit a clear trend in their locations in the HR diagram as compared to the global sample of PNe haloes as shown in Fig. 4 of CSSP03. In addition, even if the CS could be precisely located in the HR diagram, the post-AGB age at which haloes and their rings became photo-ionized cannot be accurately determined, as it depends not only on the CS mass but also on the circumstellar density distribution at the end of the AGB, which is not well known. More details about this point can be found in Perinotto et al. (2004), who showed that the post-AGB age at which the inner halo becomes photo-ionized is ~3500 yrs for a "standard" CS of $M = 0.605 \ M_\odot$ and the AGB mass distribution computed by Steffen & Schönberner (2003). The situation is more uncertain for larger masses ($M \geq 0.625 \ M_\odot$) for which this time scale would be lower although it may also happen that these haloes are never ionized.

An alternative measurement for the age of a PN is the kinematic age: its size divided by its expansion velocity. According to the models in Schönberner et al. (1997), the kinematic age of the attached shell of an elliptical PN provides a better estimate of the true post-AGB age of the nebula than that of the rim. We list on the abscissae of Fig. 3 the kinematic ages of the elliptical PNe with rings, computed for their shells using the kinematic data from the literature or from our unpublished echellograms (except for NGC 40 where no attached shell is present, we used the age of the rim instead). To compute the linear sizes, we used the distances listed in the last column of Table 2, which were determined by taking a weighted average of the values from the catalogue of Acker et al. (1992), or taken from recent papers with individual distance determinations (Reed et al. 1999 for NGC 6543 and Palen et al. 2002 for IC 2448). All nebulae
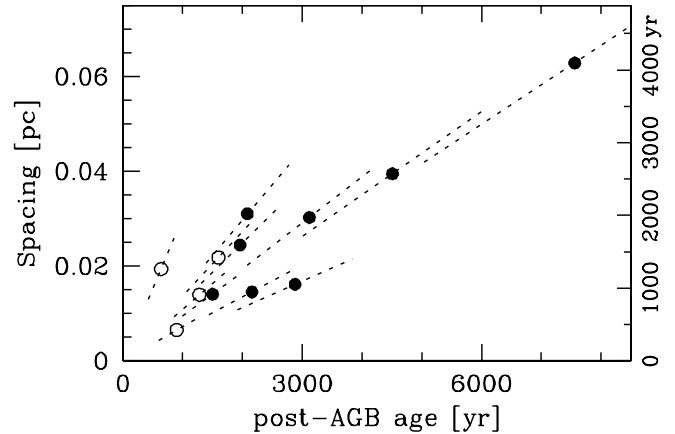

Fig. 3. Average spacing vs. the kinematic post-AGB age for elliptical PNe (filled circles) and bipolars (open circles).

except NGC 1535 (age = 7500 yrs) have kinematic post-AGB ages smaller than 4500 yrs. If we subtract from this age the time from the end of the AGB to the first photo-ionization of the halo (3500 yrs for a CS of 0.605 $M_\odot$[1]), the numbers imply that, in a broad statistical sense, the observed rings are still in the phase before they are predicted to vanish because of photo-ionization effects (MMS03). This conclusion would still hold if a slightly different distance scale, like the one in CSSP03, is adopted.

The post-AGB ages of bipolar PNe in our sample are not relevant in this discussion because their rings may not be ionized; in any case, they are all younger than two thousand years according to the adopted distances and spatiokinematic studies in the literature (Solf & Weinberger 1984; Corradi & Schwarz 1993; Guerrero & Manchado 1998; Bains et al. 2003).

5.3. Duration of the mass loss modulation producing the rings

Once the distance and expansion velocity of a PN are known, the radius of the outermost ring allows us to estimate the age of the system. We assume a halo expansion velocity of 15 km s^{-1} (see CSSP03) for all PNe, since individual kinematic measurements are mostly lacking, a general handicap when studying PN haloes.

If we subtract the "kinematic" post-AGB age of the PNe from the age of the outermost ring, we obtain an estimate of the duration of the phase of mass loss modulation at the end of the AGB producing the rings. This is shown in Fig. 4: the duration of the phase spans from 6000 yrs for IC 2448 and NGC 7009 to a maximum of 14 000–18 000 yrs for NGC 40, NGC 1535, NGC 6543 and NGC 7027. The other bipolar PNe show durations less than 5000 yrs, but they should be considered highly uncertain because the region where rings are found is very faint, and we may have missed some rings.

Therefore, since it is likely that fainter rings in other PNe in our sample were missed, we conclude that the phase of mass modulation giving rise to the rings might characterize the last

---

[1] Obviously, for post-AGB ages smaller than 3500 yrs, the photo-ionization of the halo must have occurred earlier.
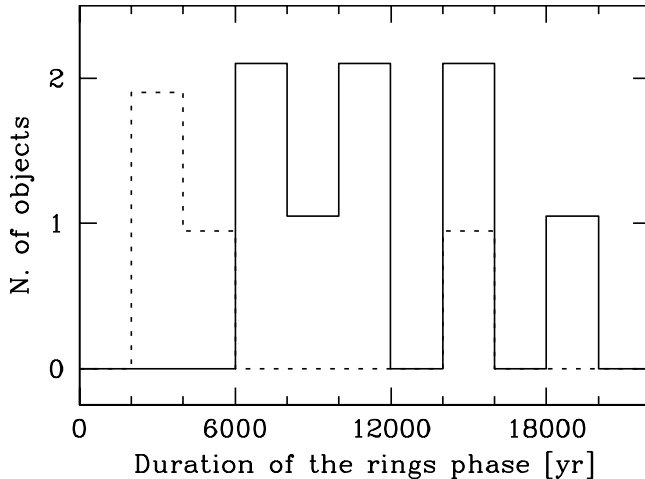
Fig. 4. Duration of the "rings" phase for elliptical PNe (solid histogram line) and bipolars (dotted line).

10 000 to 20 000 yrs of AGB evolution. CSSP03 showed in their Table 4 that for these PNe the time elapsed since the last AGB thermal pulse (whose signature is the limb-brightened edge of the AGB halo) is typically factors 1.8 to 4 longer than the ages in Fig. 4. Thus, even when we missed a few faint rings, we conclude that the formation of rings is not associated with thermal pulses.

5.4. Ring geometry and spacing

All PNe of our sample show some variation in the spacing between the rings. The most regular cases seem to be NGC 40 and NGC 7662. Most other systems of rings (Hb 5, NGC 1535, NGC 3242, NGC 3918, NGC 6543, NGC 7009) have definitely a variable spacing, with some (weak) evidence that spacing increases with distance from the central star. NGC 1535, NGC 7009 and NGC 7027 also show clear deviations from circularity, with some rings intersecting each other and in some cases with centres offset from the central star. IC 2448 and NGC 7026 have poorly defined rings and are not considered in this analysis.

The range of spacing values spanned by each system of rings is listed in Table 2. The average spacing for each PN, transformed to a linear scale using the adopted distances, is displayed in the ordinate of Fig. 3, and ranges from 0.007 pc (Hb 5) to 0.063 pc (NGC 1535). There is also an apparent trend for bipolar PNe (dotted histogram) to have smaller spacings than elliptical PNe, but this is not statistically significant because of the small sample. Adopting an expansion velocity of 15 km s^{-1}, these spacings corresponds to timescales for the mass loss fluctuations of between 400 and 4000 yr (see the right y-axis of Fig. 3).

Most interestingly, Fig. 3 shows that the average spacing correlates with the post-AGB age of the nebula, suggesting the existence of evolutionary effects in the ring spacing. This is even more clearly indicated by the fact that the spacing in the six proto-PNe listed by Su (2004) is systematically and significantly smaller than that of our sample of PNe, ranging between 80 and 600 yr if the same expansion velocity

of 15 km s^{-1} is adopted. In Fig. 3, we indicate with dotted lines how points would move if the distances were off by a factor of two (33% on each side of the adopted value). The distance enters linearly in both the estimate of the linear spacing and the kinematical age and may therefore cause a false correlation to appear. From the dotted lines it can be seen that if the distances of the three objects (NGC 1535, NGC 40 and NGC 7662) that better define the linear correlation in Fig. 3, are overestimated by a factor of $\lesssim 2$, the evidence for the existence of the correlation would be weaker. Our result should therefore be treated with some caution.

5.5. Surface brightness profiles and peak-to-continuum ratio

Radial surface brightness profiles of the inner haloes of our sample of elliptical PNe were extracted at position angles corresponding to the minor axis of the rims/shells. In most cases, a power law $I \propto r^{-\gamma}$ provides a fairly good fit to the surface brightness profiles in the region of the rings (especially for IC 2448, NGC 3242, and NGC 7662), with γ ranging from 3.3 to 4.5. In the case of IC 2448 and NGC 3242, γ decreases abruptly to shallower slopes at the end of the region occupied by the rings; in other cases, like NGC 40, NGC 1535, NGC 3918 and NGC 7009, the slope of the power-law shows a more systematic and continuous decrease with radius, and this is even more pronounced in the two PNe with no rings (NGC 6826 and NGC 2022) which we consider for comparison. These surface brightness slopes correspond to density profiles in the regions of the rings steeper than ρ^{-2}, in some cases as steep as ρ^{-3}. This confirms that mass loss increases substantially at the end of the AGB phase (e.g. Steffen & Schönberner 2003).

Once this large-scale trend was removed, we estimated the surface brightness contrast between the ring peaks and the (pseudo)continuum (or, in other words, half the contrast between the ring peaks and dips). Limited spatial resolution (through seeing or finite mirror size) reduces the true peak-to-continuum intensity contrast. An estimate of this can be found by comparing ground-based and HST data. We compared the HST ACS [OIII] images of NGC 6543 (instrumental resolution 0.″05) with those obtained at the NOT (seeing 0.″8). For different rings (whose typical width is 2″ and spacing 2.″9), the peak-to-continuum ratio in the NOT images is measured to be between 5% and 10% lower than in the HST images, where it reaches a maximum value of 1.2. In other PNe of our sample, spacing between rings is equal to or larger than that of NGC 6543, so that if the ratio between the width and spacing does not vary dramatically, we do not expect that the estimate of the peak-to-continuum ratios using our ground-based images underestimates the real values much more than the amount found for NGC 6543.

In all nebulae, we find that the peak-to-continuum intensity ratio is strongly variable within the same system of rings. The maximum peak-to-continuum ratio measured for each PN is reported in Table 2. Even considering seeing effects, these numbers are systematically lower than for the sample of

proto-PNe in Su (2004). We find however, no (anti)correlation with the kinematical post-AGB age of our nebulae. This could be explained by the large dispersion and irregularity in the peak-to-continuum contrast for individual rings within the same nebula, which make the values listed in Table 2 just an order of magnitude number. Note also that the rings in proto-PNe show up in reflected light, whereas the ionized haloes produce intrinsic emission, which may also account for some of the differences.

For bipolar PNe, reliable measurements of the peak-to-continuum surface brightness can only be done for Hb 5 and NGC 7027. The values listed by Su (2004) are also listed in Table 2.

6. Discussion, interpretation and conclusions

In spite of the paucity of data available so far, the origin of rings in PNe haloes has been widely debated, and a number of formation mechanisms has been proposed. These include binary interaction (Mastrodemos & Morris 1999), magnetic activity cycles (Soker 2000; García-Segura et al. 2001), instabilities in dust-driven winds (Simis et al. 2001) and stellar oscillations (van Horn et al. 2003; Zijlstra et al. 2002; Soker 2004). These models all produce rings morphologically similar to the observed ones, and only a detailed study of their physical and dynamical properties will allow us to distiguish the models. A first start of this was made by MMS03, who followed the evolution of rings produced by dust-driven wind instabilities using radiative hydrodynamic modelling, resulting in emission properties, line ratios, and line shapes.

The main differences between the models are in the way the rings are supported, and, at least in the published versions of the models, the amplitudes of the variations. In the case of magnetic field reversals, the rings are supported by magnetic fields, material collecting in areas of low magnetic pressure. This makes for stationary rings and the authors claim that this will provide for the required longevity. In the other cases the rings are dynamic, corresponding to waves (density and velocity variations) set up by variations in the mass loss either caused by variations at the base of the wind (dust-driven wind instabilities or stellar oscillations), or created by the interaction with a companion star. Such dynamic rings will ultimately disappear, the time scale depending on the amplitude of the waves, and the sound speed in the wind material. The latter means that this process will be slow while the wind is neutral and speed up after ionization. A simple estimate can be derived from the ratio of the extent of the ring area and the sound speed, giving values of 100 000 yrs during the neutral phase and several 1000 yrs during the ionized phase.

The distinction between magnetic and dynamically supported rings is not as clear cut as that though, since photo-ionization will raise the thermal pressure of the wind, making the magnetic pressure insignificant compared to the thermal pressure. This probably means that the evolution of the rings during the ionized phase will be similar in all models, but detailed magneto-hydrodynamic modelling should confirm this.

The simulations of MMS03 showed that the original velocity variations in the wind in case of dynamically supported winds is only important for survival of the rings during their neutral phase. Raising the pressure of the rings by photo-ionization will strengthen the waves and much higher velocity variations are then induced.

The simulations in MMS03 show a number of properties which are consistent with our new sample of rings. Firstly, the spacing of the rings tends to increase with time. This is due to the slow merging of the waves, a process which takes place from the start in the dynamically supported case, and will probably only start after ionization in the magnetically supported case. Although the indications for this in the data are not conclusive, comparing the typical spacing in the proto-PNe from Su (2004) with our PNe shows this to be significant. The models also predict a weakening of the amplitude of the rings over time, for which we also find some, albeit marginal, evidence.

As to the observed amplitudes, one should realize that the rings are not discrete entities, but rather density variations which we see in projection. It is therefore not trivial to interpret the observed values which may also be affected by temperature variations, boosting the forbidden lines of [O III] and [N II]. Taking the published results of MMS03 we see that the amplitudes are rather modest, of order 1.1 (see their Figs. 10 and 11) and therefore comparable to the observed values. The slope of the surface brightness profile seems to be shallower than in the observations, but since the average AGB mass loss was taken to be constant in the simulations, this is not surprising.

In general then, the observed properties of the rings make sense within the frame work of the dust-driven wind instability model explored by MMS03. However, as these authors pointed out, this does not necessarily mean that other models are excluded. Basically, any model which leads to dynamically supported rings can be expected to give such results, although it would be nice to see this confirmed by simulations, especially for the magnetic reversal models. In any case, all models should now face the evidence that rings are frequently found (and in all morphological classes), and the proposed formation mechanism should apply to a large fraction of AGB stars producing PNe.

Concluding, we have shown in the present paper that rings are common in PNe haloes, and thus of general relevance in the discussion of the large mass loss increase that characterises the latest AGB evolution. Testable predictions (especially in terms of the physical and dynamical properties of the rings) which are able to distinguish among all the different formation mechanisms proposed are however presently lacking, and would be highly desirable in order to allow further progress in this recent and important issue of the AGB and post-AGB evolution.

References

Acker, A., Ochsenbein, F., Stenholm, B., et al. 1992, Strasbourg–ESO Catalogue of Galactic Planetary Nebulae ESO (Garching)

Bains, I., Bryce, M., Mellema, G., Redman, M. P., & Thomasson, P. 2003, MNRAS, 340, 381

Balick, B., Wilson, J., & Hajian, A. R. 2001, AJ, 121, 354

Corradi, R. L. M., & Schwarz, H. E. 1993, A&A, 269, 462

Corradi, R. L. M., Schönberner, D., Steffen, M., & Perinotto, M. 2003, MNRAS, 340, 417 (CSSP03)

Corradi, R. L. M., Sánchez-Blázquez, P., Gianmanco, C., Mellema, G., & Schwarz, H. E. 2004, in Asymmetrical planetary nebulae III: winds structure and the thunderbird, ASP Conf. Ser., in preparation

García-Segura, G., López, J. A., & Franco, J. 2001, ApJ, 560, 928

Guerrero, M. A., & Manchado, A. 1998, ApJ, 508, 262

Mal'kov, Y. F. 1997, ARep, 41, 760

Mastrodemos, N., & Morris, M. 1999, ApJ, 523, 357

Meijerink, R., Mellema, G., & Simis, Y. 2003, A&A, 405, 1075 (MMS03)

Mellema, G. 1994, A&A, 290, 915

Palen, S., Balick, B., Hajian, A. R., et al. 2002, AJ, 123, 2666

Perinotto, M., Schönberner, D., Steffen, M., & Calonaci, C. 2004, A&A, 414, 993

Reed, D. S., Balick, B., Hajian, A. R., et al. 1999, AJ, 118, 2430

Sahai, R. 2002, RMxAC, 13, 336

Schönberner, D., Steffen, M., Stahlberg, J., Kifonidis, K., & Blöcker, T. 1997, in Advances in Stellar Evolution, ed. R. T. Rood, & A. Renzini (Cambridge Univ. Press), 146

Simis, Y. J. W., Icke, I., & Dominik, C. 2001, A&A, 371, 205

Soker, N. 2000, ApJ, 540, 436

Soker, N. 2002, ApJ, 570, 369

Soker, N. 2004, in Asymmetrical planetary nebulae III: winds structure and the thunderbird, ASP Conf. Ser., in preparation [astro-ph/0309228]

Solf, J., & Weinberger, R. 1984, A&A, 130, 269

Steffen, M., & Schönberner, D. 2003, in IAU Symp. 209, Planetary Nebulae: Their Evolution and Role in the Universe, ASP, 439

Su, K. 2004, in Asymmetrical planetary nebulae III: winds structure and the thunderbird, ASP Conf. Ser., in preparation

Terzian, Y., & Hajian, A. R. 2000, ASP Conf. Ser., 199, 34

Van Horn, H. M., Thomas, J. H., Frank, A., & Blackman, E. G. 2003, ApJ, 585, 983

Zijlstra, A., Bedding, T. R., & Matei, J. A. 2002, MNRAS, 334, 498